Reprinted from Ceramic Bulletin, Vol. 69, No. 9, September 1990

High-Resolution Ultrasonic Nondestructive Characterization

MAHESH C. BHARDWAJ*
Ultran Laboratories, Inc., State College, Pennsylvania 16801

Ultrasonic nondestructive characterization (NDC) is receiving a considerable amount of attention from the materials industry, due primarily to the current revolution in advanced materials development and the electronic, structural, and biomedical applications of these materials. To meet the challenges of materials characterization objectives, ultrasonic science and technology have also realized substantial developments in recent years.

Correlations of acoustic measurements (ultrasonic velocities, frequency dependence of ultrasound attenuation, and phase relations of reflected and transmitted ultrasonic signals) with test-material properties (density, porosity, intergranular relationships, elastic and mechanical properties) establish the basis for NDC. To exhibit the reliability of ultrasound for meaningful NDC, Vary (1987),[1] Thompson (1982–1988),[2] Kino (1987),[3] Duke (1988),[4] Bhardwaj (1987, 1990),[5,6] Liaw *et al.* (1990),[7] and others have demonstrated advancements in time- and frequency-domain analysis of a wide range of industrial materials and components. Although the advantages of NDC are numerous and evident, it is still a relatively new subject. Ultrasonic characterization is a science-intensive discipline; therefore, it is imperative to perceive it in light of other methods that also use a wave as the characterizing vehicle. Ultrasonic methods and experimental techniques for characterizing materials properties and microstructure need to be developed further.

Ultrasonic Resolution

Resolution is the ability of an ultrasonic wave to distinguish two closely lying planes such as the top and bottom surfaces, or test surface and internal defect/discontinuity in a test material. In time domain, top and bottom surfaces are indicated by the incident and reflected ultrasonic signals, respectively. Measurement of time-of-flight (TOF) between these signals can be used to locate a discontinuity with respect to its distance from the test-material surface through which ultrasound is propagated. Resolution of these signals can also be used to conduct internal imaging by monitoring the amplitude or TOF of the reflected signal, to investigate interfacial phenomena in multilayered materials, and to determine the velocity of ultrasound (if thickness is known) and thickness of test material (if velocity is known).

$$v = d/t \tag{1}$$

where v is material velocity and t is the TOF through a thickness d. The minimum thickness that an ultrasound wave can resolve in a given material is defined by

$$d_{min} = n\lambda/2 \tag{2}$$

where n is the number of wavelengths (λ) of the interrogating wave.

Since the objective is to distinguish between the top and bottom surfaces or between the test surface and an internal discontinuity in a test material in time domain, it is more convenient to express interrogating frequency and its wavelength in time units. For example, at 10 MHz, $1\lambda = 100$ ns, $2\lambda = 200$ ns, and so on. Figure 1 shows idealized time-domain envelopes of these waves. Wavelength, here, refers to the period of incident ultrasound:

$$P(\lambda) = 1/f \tag{3}$$

where f is the frequency of incident wave. Time (period) and distance (wavelength) can be interchanged to define either the distance between test-material surfaces, or TOF between them.

Significance of Incident Time-Domain Envelope

Consideration of the size of time-domain envelope of an incident ultrasonic wave, i.e., the amount of its vibration with respect to travel time through a test medium, is of paramount importance in determining its (incident wave) suitability for a given resolution requirement. For example, if TOF through a test material is 200 ns, then its top and bottom surfaces can be resolved by a 1λ 10-MHz ultrasonic wave. Despite the frequency, a 2λ ultrasonic pulse is expected to yield poor-to-marginal resolution, and a 3λ pulse will produce no resolution at all. Obviously, because of the excessive vibration, 200- and 300-ns incident pulses will interfere with the reflection of a bottom surface signal lying 200 ns away from the top surface. These relations are idealized in Figs. 2 and 3. Figure 2 shows the wave-propagation sequence of three selected pulses,

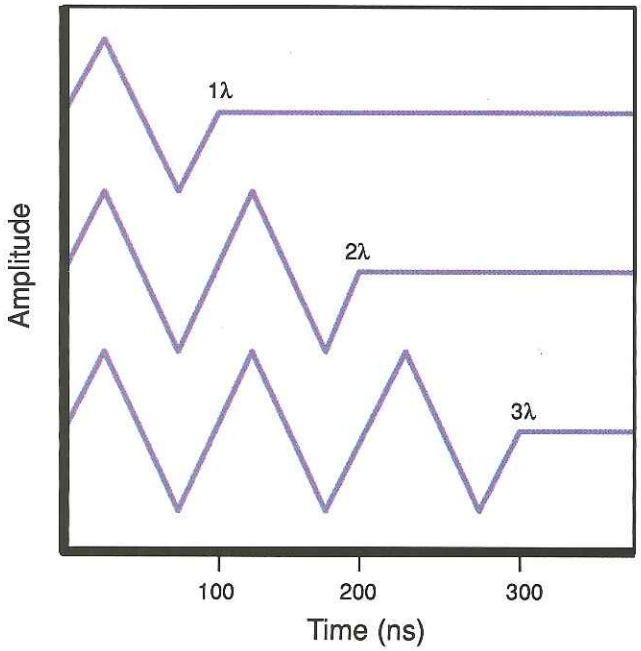

Fig. 1. Idealized representation of 10-MHz 1λ, 2λ, and 3λ wavelength ultrasonic time-domain envelopes.

*Member, American Ceramic Society.

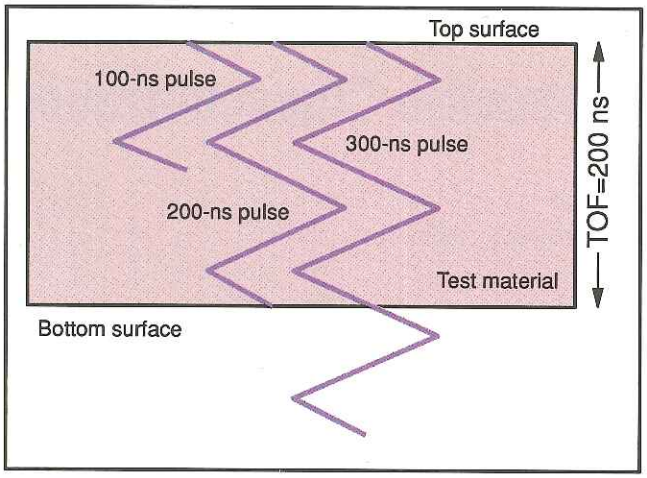

Fig. 2. Schematic wave-propagation sequence of 100-, 200-, and 300-ns ultrasonic pulses through a test material of 200-ns TOF.

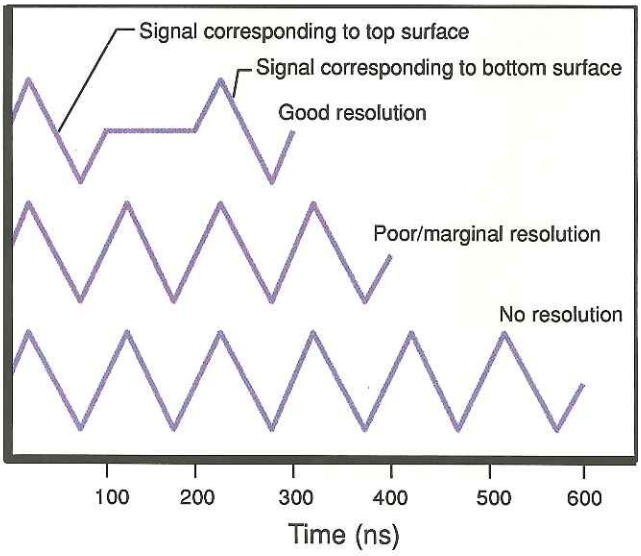

Fig. 3. Idealized or expected time-domain traces from the interrogation of 100- (top trace), 200- (middle trace), and 300-ns (bottom trace) ultrasonic pulses through a test material of 200-ns TOF.

whereas Fig. 3 shows the expected time-domain traces from these pulses through the test material of 200-ns TOF.

Figure 4 is a near-perfect simulation of a real example of 100-, 200-, and 300-ns interrogating pulses of ultrasound through a specimen of steel plate (0.6 mm thick and 5970 m/s ultrasonic velocity) with 200-ns TOF. This experiment proves that resolution by a 100-ns pulse (top trace) is excellent, a 200-ns pulse (middle trace) is poor or marginal at best, and resolution with a 300-ns pulse (bottom trace), is not discernible with a 0.6-mm steel plate.

From the foregoing discussion, the following conclusions can be made.

(a) At a specified ultrasonic frequency, the pulse width (time-domain envelope or packet) determines the suitability of resolution in a given material with respect to TOF of the propagating ultrasound in the material.

(b) If the pulse width of incident ultrasound (even when attempts are made to increase resolution through increased frequency) is large, compared with the actual TOF in a given material, then the resolution of the top and bottom surfaces of the material is not feasible. For example, if a 20-MHz-frequency ultrasound of a 200-ns pulse is used for the characterization of a 0.6-mm steel plate, then the ensuing result will most likely correspond to the middle trace of Fig. 4.

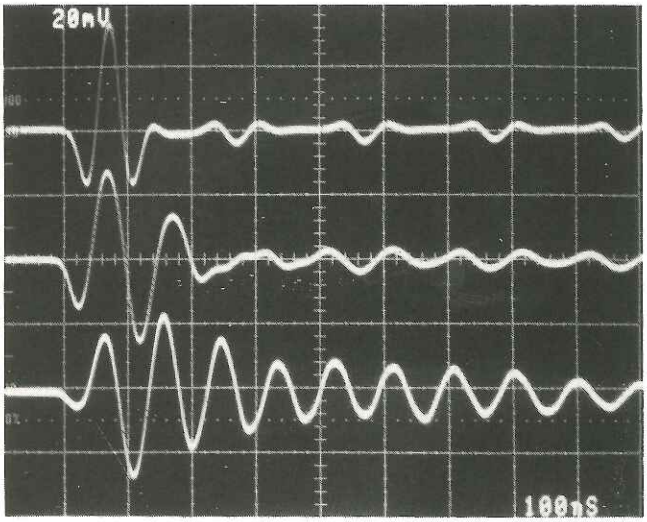

Fig. 4. Real example of time-domain traces from approximately 100- (top trace), 200- (middle trace), and 300-ns (bottom trace) ultrasonic pulses through a test material with 200-ns TOF. Extreme left signal corresponds to the top surface of the specimen as well as to the actual pulse shape and size of the incident ultrasound. Signal immediately following that of the top surface corresponds to that of the bottom test material surface. Rest of the right-hand signals represent multiple reflections of ultrasound through the specimen.

Table I. Minimum Resolvable Thicknesses and Spatial Resolution in Selected Materials (Defined by Ultrasonic Velocities) as Functions of Incident Pulse Widths

	d_{min} (mm)*											
	Incident Frequency (10 MHz)				Incident Frequency (20 MHz)				Incident Frequency (50 MHz)			
	Pulse width (ns)				Pulse width (ns)				Pulse width (ns)			
Velocity (m/s)	0.5λ† (50)	1λ (100)	2λ (200)	3λ (300)	0.5λ† (25)	1λ (50)	2λ (100)	3λ (150)	0.5‡ (10)	1λ (20)	2λ (40)	3λ (60)
6000§	0.15	0.3	0.6	0.9	0.075	0.15	0.3	0.45	0.03	0.06	0.12	0.18
12000¶	0.3	0.6	1.2	1.8	0.15	0.3	0.6	0.9	0.06	0.12	0.24	0.36

*Minimum thickness that can be resolved when direct-reflection technique is used. TOF corresponds to "round-trip" through test material. †0.5 to 0.75 wavelength pulse widths are possible from "critically" damped and acoustically matched lambda and piezo-film transducers. ‡At the time of this writing, half wavelength pulse width at 50 MHz is unknown. §Materials such as fibrous and particulate ceramic composites, powder metals, medium-porosity ceramics, steels, aluminum, etc. ¶Materials such as dense oxides, carbides, nitrides, and borides of metals and nonmetals, diamond, sapphire, etc.

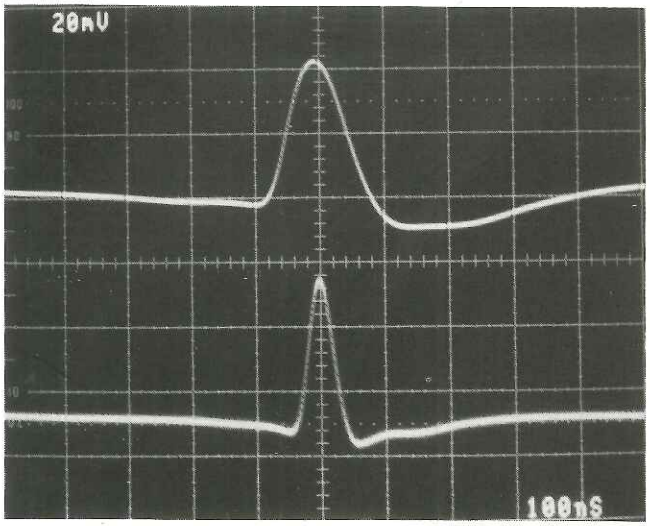

Fig. 5. Typical pulse widths of focused λ transducers. Top trace: nominal frequency is 5 MHz, active area diameter is 12.7 mm, and focal length in water is 6.3 cm. Measured pulse width is ≈150 ns. (Theoretical minimum pulse width (λ/2) at 5 MHz is 100 ns.) Bottom trace: nominal frequency is 10 MHz; active area diameter is 6 mm; and focal length in water is 1.9 cm. Measured pulse width is ≈55 ns. (Theoretical minimum pulse width (λ/2) at 10 MHz is 50 ns.)

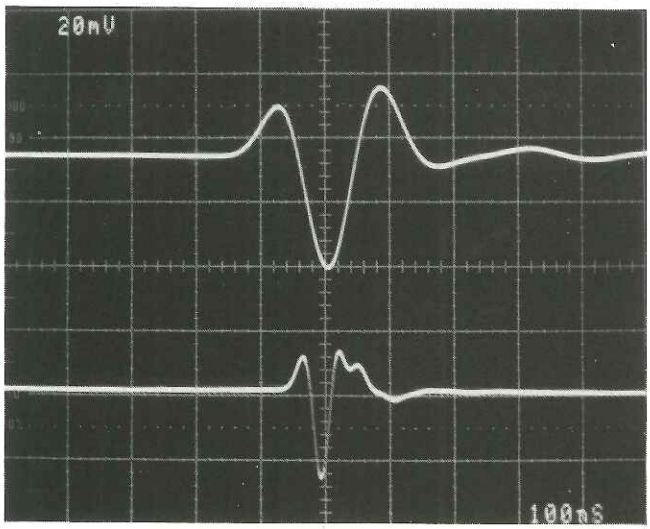

Fig. 6 Typical pulse widths of planar λ transducers. Top trace: nominal frequency is 5 MHz and active area diameter is 12.7 mm. Measured pulse width is ≈160 ns. (Theoretical minimum pulse width (λ/2) at 5 MHz is 100 ns.) Bottom trace: nominal frequency is 10 MHz and active area diameter is 6 mm. Measured pulse width is ≈70 ns. (Theoretical minimum pulse width (λ/2) at 10 MHz is 50 ns.)

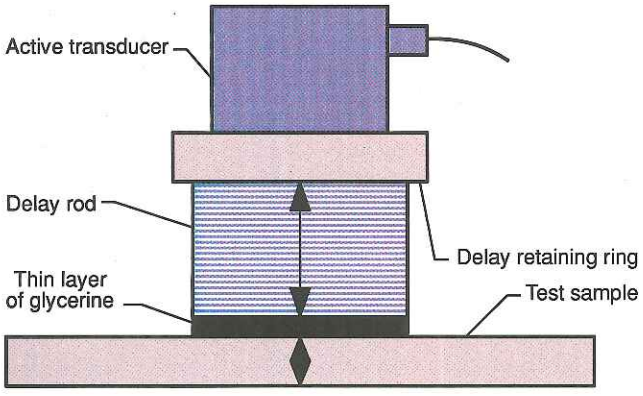

Fig. 7. Coupling of a delay line λ-series transducer to the test-material surface used for the demonstration of high resolution without VHF.

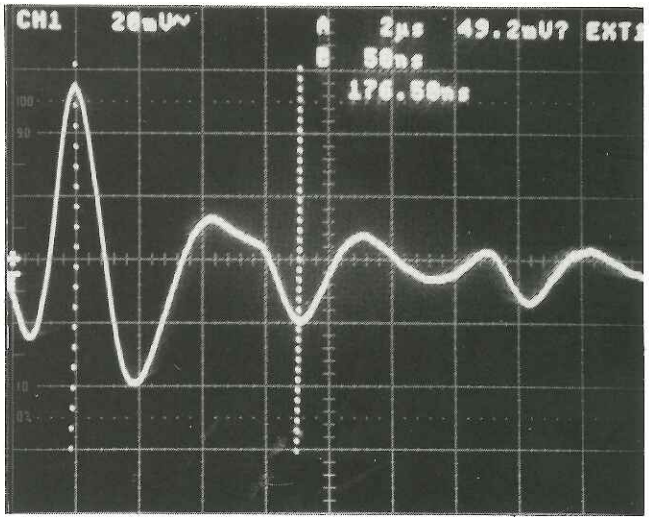

Fig. 8. Resolution (100%) of top and bottom surfaces of a 1.0-mm-dense BeO substrate obtained by a delayed contact λ-series transducer (10-MHz nominal frequency and 6-mm active area diameter). Left-hand cursor is at the delay–BeO interface; right-hand cursor is at BeO–ambient interface. Measured TOF is 176.5 ns; measured velocity of ultrasound is 11 330 m/s.

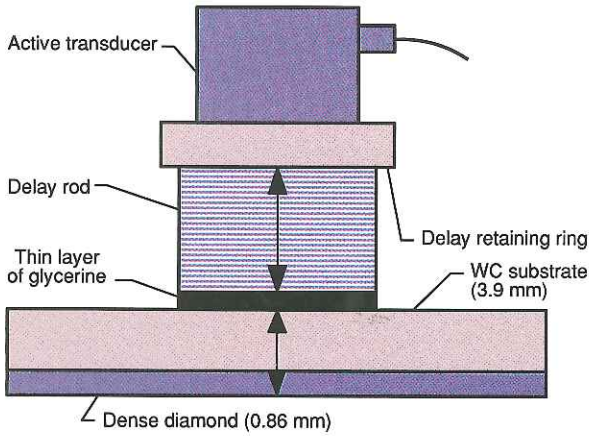

Fig. 9. Coupling of a delay line λ-series transducer to a diamond-deposited WC tool showing the critical dimensions of the test sample.

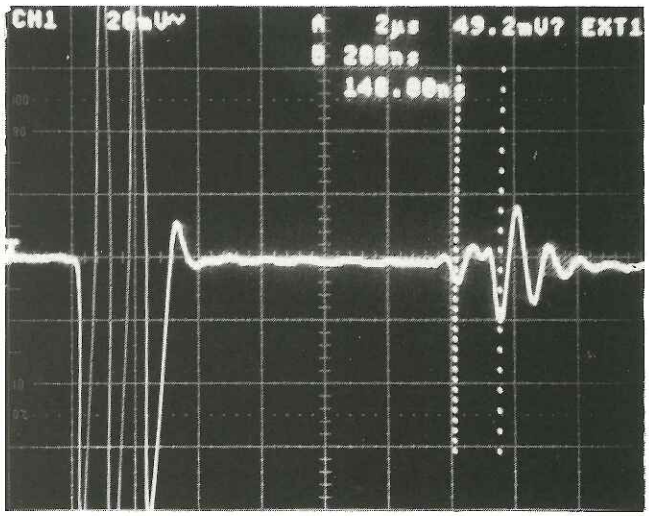

Fig. 10. Ultrasonic observations from the test setup shown in Fig. 9. Data were acquired by a delayed-contact λ-series transducer (20-MHz nominal frequency and 3-mm active area diameter). Extreme left is transducer delay–WC interface; second from left is WC–diamond interface; and extreme right is diamond–ambient interface. Measured WC TOF is 1.14 µs and velocity is 6840 m/s. Measured diamond TOF is 140 ns and velocity is 12 285 m/s.

It is now clear that the most important parameter defining resolution is the width of the ultrasonic pulse. Therefore, a practical definition of resolution by ultrasound must contain a term that specifies the pulse width.

$$d_{min} \geq p \quad (4)$$

where p is the actual width of an interrogating/incident ultrasonic envelope, and where d_{min} is also translated into time units (Eq. (1)). Or, for optimum resolution

$$p < M_{TOF} \quad (5)$$

where M_{TOF} is the known TOF through the test material.

For example, to characterize 1-mm-thick dense Si_3N_4 (12 000 m/s ultrasonic velocity) by direct-reflection technique, the width of the ultrasonic pulse must be <165 ns, since the round-trip of TOF of this material is 165 ns. Similarly, to resolve the interface between a dense diamond coating (0.5 mm, 12 500 m/s ultrasonic velocity) on a WC substrate from the diamond side, the pulse width of incident ultrasound must be <80 ns. Table I provides a list of resolution limits, d_{min}, for two material categories defined by ultrasonic velocities as functions of incident pulse widths. Experience also shows that indiscriminate increment of frequency for higher resolution does not necessarily yield the desired result in all materials. Higher frequencies do not automatically produce reduced pulse widths or higher resolutions. Consider the following:

(a) Most high-frequency transducers (>30 MHz) are characterized by more than 2λ pulse widths.

(b) Asymmetrical pulse shapes and distorted frequency-domain characteristics of poorly designed transducers (>30 MHz) are well-known. The combined effects of such transducers with most commercial ultrasonic excitation and amplification systems generally yield reduced frequency response to an otherwise high-frequency transducer. Reduced frequency means increased pulse width and thus poor resolution.

(c) According to the frequency dependence of ultrasonic attenuation, it is universally true that beyond a certain frequency (optimum frequency), attenuation increases exponentially in the media through which ultrasound is propagated. Ultrasonic investigation shows that dense oxides, carbides, nitrides, and borides of metals and nonmetals, and materials such as sapphire, quartz glass, and most single crystals (based upon ceramic starting ingredients) are relatively acoustically transparent over a wide range of frequencies. However, porous and granular materials are attenuated more rapidly at higher frequencies. Therefore, indiscriminate increment of frequencies, i.e., without the consideration of a test material's frequency-dependence characteristics, will most likely yield reduced signal strengths, low signal-to-noise ratios, and poor resolution.

High Resolution without Very High Frequency

As further advances have been made in the science and technology of very high frequency (VHF) ultrasonics, it has become feasible to conduct relatively high-resolution NDC. As shown in the preceding discussion, if the pulse width of incident ultrasound at a specified frequency is reduced well below one or two wavelengths, then resolution can be dramatically improved. This can be achieved through "critical" damping and "specific" acoustic impedance matching of piezoelectric transducers.[8] By using a broadband amplifier and a short pulse -ve spike or square-wave excitation system, these devices generate near perfect λ/2 impulses in spherically focused designs (Fig. 5) and <1λ pulse widths in planar designs (Fig. 6).

Devices based upon these designs have been developed from <200 kHz to ≈30 MHz. Specific acoustic impedance matching from high (43×10^5 g/(cm^2·s)) to low (1.5×10^5 g/(cm^2·s)) has also been achieved in short-pulse devices. These considerations, besides facilitating high resolution, also allow "optimum" transmission of ultrasound through a variety of materials varying in composition and microstructure. To characterize relatively porous and liquid-sensitive materials, a dry-coupling mechanism has also been implemented in such transducers. The combination of high-resolution (high-bandwidth) and materials-suitable (dry-coupling)[6] methodology has been successfully applied to the bulk NDC of superconducting materials.[9]

Applications of Short-Pulse Ultrasonics in NDC

In the following paragraphs, some significant NDC applications of short-pulse impedance-matched transducers on selected materials are described. While performing these applications, rf A-scans were obtained by excitation of transducers with a short-duration (<50 ns) -ve square-wave pulser and amplification by a broadband amplifier (1000 Hz to 30 MHz). Ultrasonic images were generated by monitoring transmitted ultrasonic signals through test materials by computer-controlled raster scanning of transducers in water. The acquired image data were further enhanced by the image-processing software.

To demonstrate the applicability of the extraordinary resolution capabilities of λ-series ultrasonics, a delayed 10-MHz and 6-mm active area transducer was used. The physical arrangement of the transducer with the test material is shown in Fig. 7. Since only dense and impervious materials were examined here, a thin layer of glycerine was used as a coupling agent between the delay rod and the test material.

Figure 8 is a time-domain oscilloscope trace obtained from 1.0-mm-thick BeO substrate by the direct-reflection method with a delayed 10-MHz and 6-mm active area diameter, λ-series transducer. Observe the complete resolution of the top and bottom surfaces of this material. This is represented by signals corresponding to the delay–top surface interface (extreme left indication) and the bottom surface–ambient interface (middle indication). (In Fig. 8, the left-hand cursor is 11 330 m/s.) Since the pulse width of the transducer used is short enough, even thinner samples of BeO or similar materials can be reliably examined by using this method. Considering the fact that dense oxides, carbides, nitrides, and borides are typically long-wavelength materials (BeO at 10 MHz being 1.13 mm), it is particularly encouraging to note that the relatively low 10-MHz frequency (of very short pulse width) enables extraordinary high resolution without the applications of VHF. By using dry-coupling designs of λ-series transducers, the same results are obtained with virtually no reduction in resolution.

To characterize a thin coating of diamond deposited on a WC substrate in a drilling tool, an arrangement similar to the one shown in Fig. 7 was used. Ultrasound from a delayed 10-MHz and 6-mm active area diameter λ-series transducer was propagated from the WC side, as shown in Fig. 9. The resulting ultrasonic signal is shown in Fig. 10. Here, the left cursor is at the WC–diamond interface and the right cursor is at the diamond–ambient interface. The round-trip TOF through 0.86-mm-thick diamond is 140 ns, yielding 12 285 m/s velocity of longitudinal waves. It is important to note that despite low (3%) reflectivity at the diamond–WC interface, the quality of signal is good enough for its interpretation.

Transducer coupling to a multilayer ferrite composite, investigated for interfacial quality at the glass–$BaTiO_3$ interface is shown in Fig. 11. Figure 12 shows A-scans from bonded (top trace) and partially bonded (bottom trace) conditions of $BaTiO_3$ with glass in a multilayer ferrite composite. These data were obtained by a delayed λ-series transducer, 6-mm active area diameter and 10-MHz nominal frequency. Note that when $BaTiO_3$ and glass (0.4 mm) are bonded (top trace), the interface (left indication) is clearly defined from the bottom surface of the glass (right indication). When there is a partial or complete disbond at the glass–$BaTiO_3$ interface, most of the ultrasonic energy is reflected directly from it, thus minimizing the reflection from the glass–ambient interface (Fig. 11, bottom trace). It is important to note that the reflection coefficient at the glass–$BaTiO_3$ interface

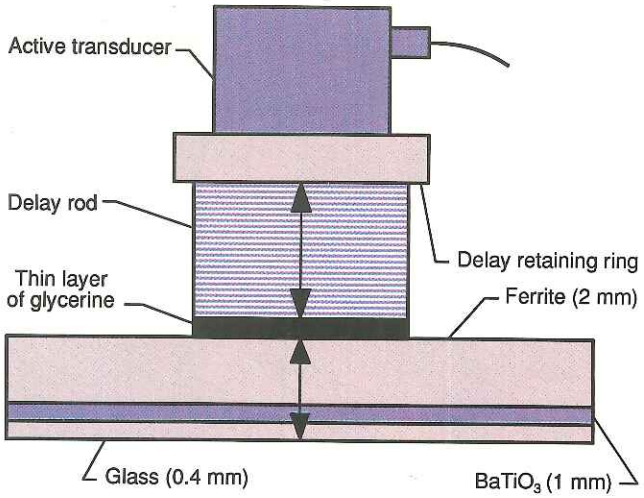

Fig. 11. Transducer to a multilayer ferrite composite relationship used for the characterization of $BaTiO_3$–glass interface.

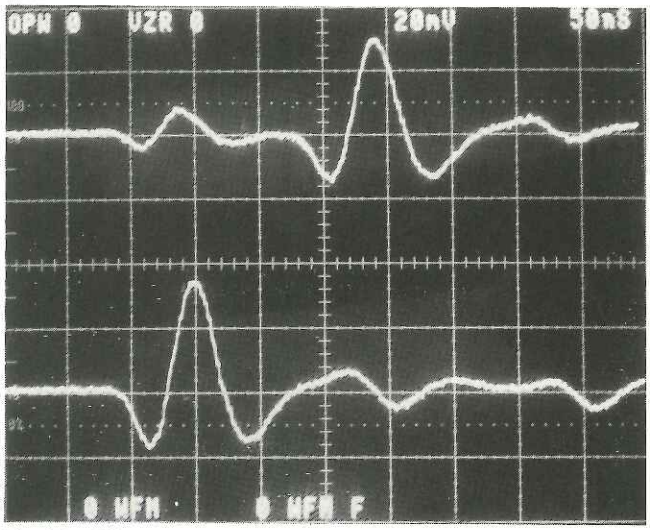

Fig. 12. Ultrasonic observations from the test setup shown in Fig. 11. Data were acquired by a delayed contact λ-series transducer (10-MHz nominal frequency and 6-mm active area diameter). Since the object of this investigation was to characterize bond quality at $BaTiO_3$–glass interface, only signals corresponding to it and to the bottom surface of glass are shown here. Top trace is defect-free or "good" bond-quality region. Left signal corresponds to $BaTiO_3$–glass interface; right signal is from glass–ambient (bottom surface) interface. Bottom trace is defect or partially bonded region. Amplitude of $BaTiO_3$–glass interface is higher than the one in the top trace, while that of the glass–ambient is lower. This observation indicates that because of the disbonding of this interface, most of the ultrasonic energy is reflected from it, thus the higher amplitude.

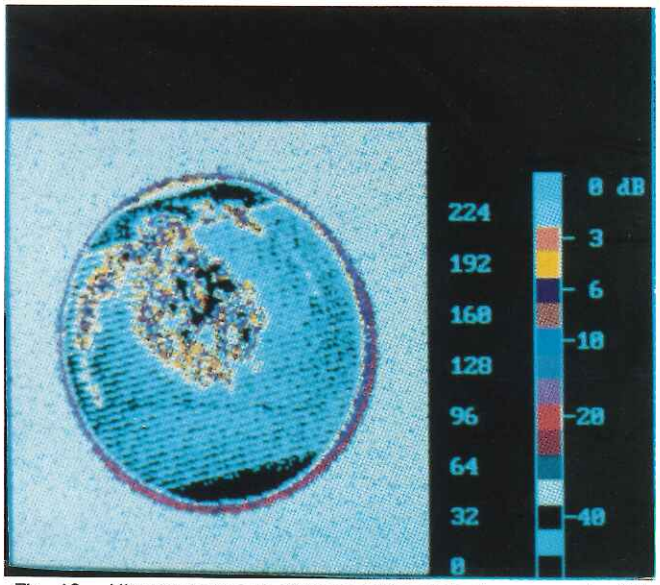

Fig. 13. Ultrasonic image of the multilayer ferrite composite (10-cm diameter and ≈4-mm thick) examined by A-scan, Fig. 12. Data were acquired by a water immersion λ-series transducer (10-MHz nominal frequency, 6-mm active area diameter, and 1.9-cm point focused in water). Upper-left-hand and center portions of figure corresponds to the defects observed in Fig. 12. Lines in figure correspond to the surfacial features of this material.

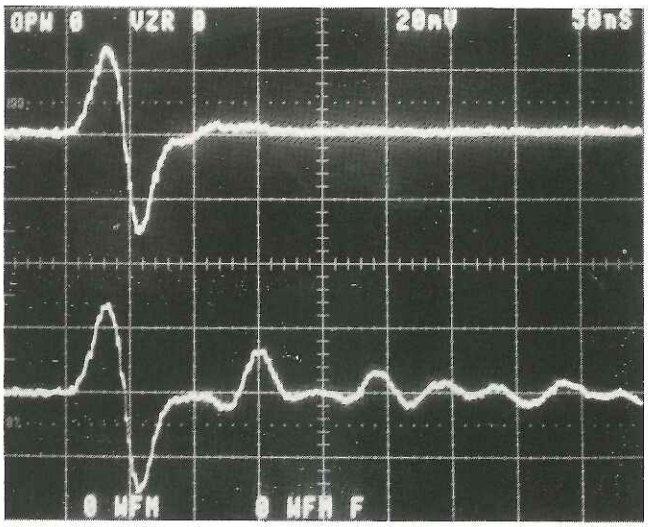

Fig. 14. Simultaneous high resolution and defect detectability by using the water immersion method with a 10-MHz, 6-mm active area diameter, and 1.9-cm λ-series transducer. Test sample used for this demonstration is an aircraft-quality aluminum with an artificial 1-mm defect located at 0.4 mm from the test surface. Top trace: signal corresponding to water–aluminum interface in the defect-free region. Bottom trace: signal corresponding to the reflection (also multiple reflections) from the shallow subsurface defect.

is only 2%. Despite this apparently low reflectivity, a "clean" ultrasonic signal is observed from this interface.

This material was also examined by ultrasonic imaging by using a λ-series 10-MHz, and 19-mm focused transducer. Figure 13 shows the damaged region (upper left-hand and central portions) characterized by a poor bond at the glass–$BaTiO_3$ interface, also reported in Fig. 12.

To demonstrate simultaneous resolution and detectability of very shallow subsurface defects, an artificial defect (1.0-mm diameter, located at 0.25 mm in an aircraft-quality aluminum) was characterized. This was accomplished by the water delay or immersion method, using a λ-series transducer of 10-MHz frequency, 6.0-mm active area diameter, and 19-mm point focus in water. The top trace in Fig. 14 corresponds to the defect-free region in the test sample, showing only the water–aluminum interface. The bottom trace clearly demonstrates the appearance of the shallow subsurface defect along with several reflected multiples.

Figure 15 is an example of heterogeneity in a ceramic (in this case a 92.3% sintered alumina) determined by attenuation ultrasonic imaging. Observe the subtle density variations enhanced by colored rings. If the density of the yellow bands is 92.3%, then the digitally determined value of the less dense green region is approximately 83%. Similar investigations of ceramics have been reported by

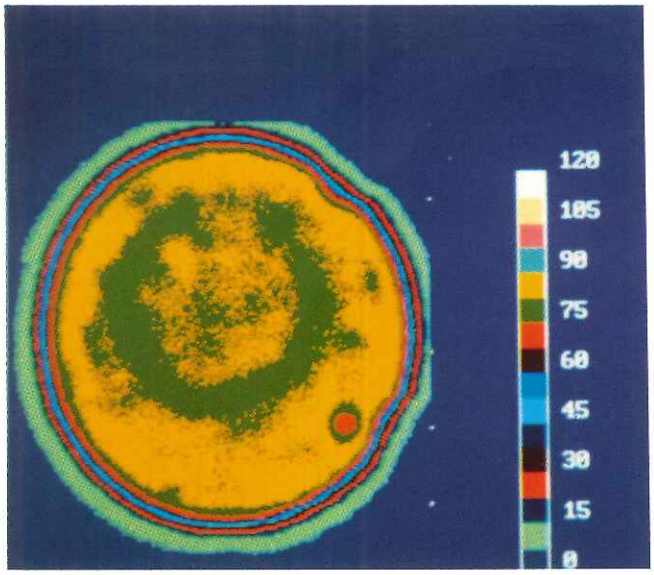

Fig. 15. Computer-enhanced ultrasonic image of a 5.1-cm-diameter and 1.3-cm-thick specimen of 92.3% dense Al_2O_3. Data were acquired by a water immersion λ-series transducer (5-MHz nominal frequency, 12.7-mm active area diameter, and 7.6-cm point focused in water). Varied colored rings are presumably indicative of density variations in this material. At the lower-right-hand portion there is an indication of a large void, ≈1 mm in diameter.

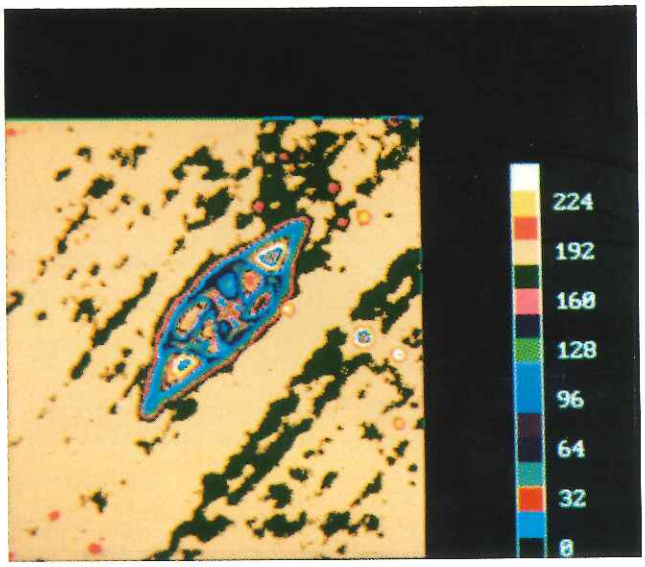

Fig. 16. ULTIMAGE-refined image of an impact-damaged graphite-fiber-reinforced epoxy composite, 13 mm × 13 mm × 1.4 mm. Green lines correspond to graphite fibers; the central region describes the geometry of the damaged area in this sample. Data were acquired by a water immersion λ series transducer, 5-MHz nominal frequency, 6-mm active area diameter, and 2.5-cm point focus in water.

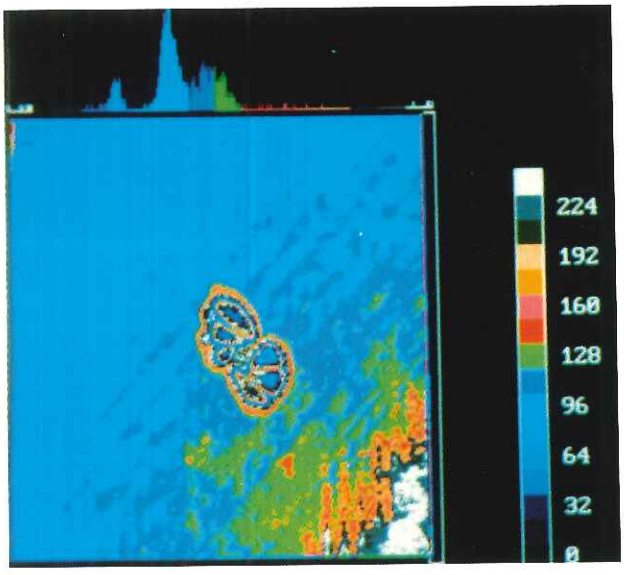

Fig. 17. Ultrasonic image of the internal region of the specimen analyzed in Fig. 16. Data were acquired by monitoring ultrasonic scatter from the inner portion of the test sample. If Fig. 16 is assumed to be the integrated or composite image of this specimen, then this figure shows the geometry of impact-damaged area only in the inner region (≈0.7 mm) of this material.

Generazio *et al.* (1988)[10] by using very high ultrasonic frequencies.

Figure 16 is a digitally enhanced ultrasonic image of a 1.4-mm-graphite-fiber-reinforced plastic composite artificially damaged by impact. This analysis was performed by monitoring the reflection of ultrasound from the far side of the test sample. Observe the clean demarcation of the impacted region's geometry with the appearance of fiber orientation. Figure 17 shows the results of the same specimen, but in this case the internal scatter from the sample was monitored while acquiring the data. The geometry of impact damage in this case corresponds to the inner region of the composite. Figure 17 further reveals fiber damage and delaminations in the inner region of this sample.

Pulse Width is Critical

In light of the relative novelty of NDC, the significant elements and requirements for high-resolution ultrasonics of materials have been defined. To conduct high resolution for TOF measurements or for detection and location of internal discontinuities in materials, it is suggested that a transducer and an ultrasonic system be specified with respect to the pulse width

of an interrogating ultrasonic wave. Mere specification of the applicable frequency is not sufficient for high-resolution NDC. Since ultrasound is capable of providing useful information about a wide range of materials, varying in composition and microstructure, it is important to consider wave-material interaction phenomena. Indiscriminate increment of incident frequency, i.e., without some idea of frequency dependence of ultrasonic attenuation with respect to a test material's characteristics, can generate undesirable results. To enhance the resolution and the accuracy of ultrasonic measurements, attempts should be made to use and generate the shortest possible ultrasonic pulses.

References

[1]Materials Analysis by Ultrasonics; Edited by A. Vary. Noyes Data Corp., Ridge Park, NJ, 1987.

[2]Review of Progress in Quantitative Nondestructive Evaluation, Vols. 1–7. Edited by D. O. Thompson and D. E. Chimenti. Plenum Press, New York, 1982–1988.

[3]G. S. Kino, Acoustic Waves, Devices, Imaging, and Analog Signal Processing. Prentice-Hall, Englewood Cliffs, NJ, 1987.

[4]J. C. Duke, Jr., Acousto-Ultrasonics, Theory and Applications. Plenum Press, New York, 1988.

[5]M. C. Bhardwaj, "Fundamental Developments in Ultrasonics for Advanced NDC"; pp. 472–527 in the Proceedings of the Joint Conference on Nondestructive Testing of High-Performance Ceramics, August 25–27, 1987, Boston, MA. American Ceramic Society, Westerville, OH, 1987.

[6]M. C. Bhardwaj, "Simple Ultrasonic NDC for Advanced Ceramics Development and Manufacture"; pp. 509–24 in Metal and Ceramic Matrix Composites. Edited by R. B. Bhagat, A. H. Clauer, P. Kumar, and A. M. Ritter.

[7]P. K. Liaw, R. E. Shannon, and W. G. Clark, Jr., "Correlation of Microstructural Characterization with Nondestructive Evaluation of Al/SiC Metal-Matrix Composites"; pp. 581–616 in Fundamental Relationships Between Microstructures and Mechanical Properties of Metal-Matrix Composites. Edited by M. M. Gungor and P. K. Liaw. The Minerals, Metals, and Materials Society, Warrendale, PA, 1990.

[8]Ultran Laboratories, Inc., "Lambda Transducers: Their Features and Applications in Nondestructive Characterization of Materials," Tech. Rept. No. EPN 104, Ultran Laboratories Publication, State College, PA, 1982.

[9]M. C. Bhardwaj, K. Trippett, and A. S. Bhalla, "Microstructure Characterization of Superconductors by Wideband Ultrasonic Spectroscopy"; presented at the 1st International Ceramic Science & Technology Congress, Anaheim, CA, November 2, 1989 (Symposium on Superconductivity and Ceramic Superconductors, Paper No. 56-SXII-89C).

[10]E. R. Generazio, D. J. Roth, and G. Y. Baaklini, "Acoustic Imaging of Subtle Porosity Variations in Ceramics," *Mater. Eval.*, **46** [10] 1338–43 (1988).